A Digital speckle stereo matching algorithm based on epipolar line correction

Liping Liu

liuliping_tj@163.com

Civil Aviation University of China

Boya Niu

AVIC Xi'an Aircraft Industry (Group) Co., Ltd

Zhuo Xu

COMAC Shanghai Aircraft Manufacturing Co., Ltd

Songyang Zhang

Civil Aviation University of China

Zhaoyu Shao

Aero Engine Corporation of China - Commercial Aircraft Engine Co., Ltd

Xinyu Wang

Civil Aviation University of China

Research Article

Keywords: Digital speckle, Inclined field of view, Deformation strain measurement, Estimation of deformational iterative initial value, Matching success rate

Posted Date: November 30th, 2023

DOI: https://doi.org/10.21203/rs.3.rs-3671043/v1

Additional Declarations: Competing interest reported. The authors declare the following financial interests/personal relationships which may be considered as potential competing interests: Liping Liu has patent #CN202310496200.X issued to China National Intellectual Property Administration. If there are other authors, they declare that they have no known competing financial interests or personal relationships that could have appeared to influence the work reported in this paper.

Version of Record: A version of this preprint was published at Signal, Image and Video Processing on March 16th, 2024. See the published version at https://doi.org/10.1007/s11760-024-03096-2.

A Digital speckle stereo matching algorithm based on epipolar line correction

Liping Liu[1], Boya Niu[2], Zhuo Xu[3], Songyang Zhang[1], Zhaoyu Shao[4], Xinyu Wang[1]

1 School of Aerospace Engineering, Civil Aviation University of China, Tianjin 300300, China

2 AVIC Xi'an Aircraft Industry (Group) Co., Ltd, Xi'an 710089, China

3 COMAC Shanghai Aircraft Manufacturing Co., Ltd, Shanghai 200126, China

4 Aero Engine Corporation of China - Commercial Aircraft Engine Co., Ltd, Shanghai 200241, China

Abstract: When the digital speckle correlation method takes images in some working conditions, the left and right images appear weak correlation due to the extreme inclination of the camera, which leads to the difficulty of matching. In order to solve the above problem, a digital speckle stereo matching algorithm based on epipolar correction is proposed in this paper, and an estimation method of deformational iterative initial values of the first-order shape function in the stereo matching process is given through theoretical derivation. The Newton-Raphson (NR) method can be directly used for fine matching in the original left and right images through the estimated deformational iterative initial value. The digital speckle matching experiment under different camera inclination angles of 24.2°, 34.2°, 41.15°, 47.3° and 52.4° is carried out to verify the effectiveness of the digital speckle stereo matching algorithm based on epipolar correction. The experimental results show that this method can complete the matching well under different inclined field of view, and the matching success rate is close to 100%, which can at least meet the requirement of digital speckle matching and deformation strain measurement under the inclination angle less than 52.4° field of view.

Key words: Digital speckle; Inclined field of view; Deformation strain measurement; Estimation of deformational iterative initial value; Matching success rate

1. Introduction

Digital Image Correlation (DIC) has been found widespread applications in various fields such as geomechanics, aerospace, biomechanics, bridge construction, and the automotive industry due to its advantages including non-contact, full-field measurement, simple optical setup, and high accuracy[1-5]. This method involves correlating and calculating the speckle patterns in the left and right images before and after deformation of the test surface to obtain the surface deformation field to be measured[6]. Generally, DIC achieves matching of corresponding points between the left and right images through coarse and fine matching processes. Successful correlation matching demands speckle images with sufficiently rich details and accurate initial values for iterations. In certain measurement conditions, influenced by the measurement environment [7], situation arises that the camera is significantly tilted. This leads to feature compression in the left and right images, substantial deformations in corresponding sub-regions, and consequently, a weak correlation between the left and right images. This weak correlation phenomenon will make both coarse and fine matching extremely difficult, ultimately resulting in a bottleneck for the DIC at the matching stage. Therefore, researching techniques to enhance the robustness of stereoscopic matching for

✉Liping Liu
liuliping_tj@163.com

digital speckle images under inclined field of view, increase the success rate of matching, and ensure matching precision, is an important issue in the field of engineering.

The Newton-Raphson (NR) algorithm[8] is a classic fine matching method in the realm of digital image correlation. It operates on an iterative principle, constantly adjusting the shape function to achieve alignment between reference and target sub-regions. The NR method is highly sensitive to initial values for iterations, and the convergence of its computations heavily relies on the accuracy of these initial values[9]. Generally, it's only suitable for cases where the image inclination angle is below 12°[10]. Enhancing the success rate of the NR method can be achieved by improving the precision of the initial values used during the iteration. Wei Bin[11] et al employed a seed point growth strategy to provide deformation iterative initial values for detection points, thereby improving the matching success rate. However, this approach neglects the matching issues of the seed points themselves. If seed point matching fails, subsequent matching becomes unfeasible. Hongying Zhang[12] assumed the deformation between left and right images was a homography transformation. They applied the improved Scale Invariant Feature Transform (SIFT) matching algorithm to estimate homography matrices through extracting the information from circular markers affixed to the object surface. Subsequently, the initial deformation value of the whole sub-region was estimated by homography matrix. However, when the inclination angle exceeded 20°, marker recognition became difficult, and feature detection became time-consuming, particularly for larger measurement areas. Ye Meitu [13] et al proposed a discretized matching approach based on the rule that the sub-region is less affected by the tilt. They decomposed the large sub-regions around seed points into smaller sub-regions for matching. After completing matching for these smaller sub-regions, the deformation of the larger sub-regions was estimated. However, these smaller sub-regions often lacked sufficient features for successful matching. This method was applicable only when speckle quality was fine. When inclination angles greater than 35.65°, the success rate of matching for the smaller sub-regions didn't exceed 10%, causing limitations in the selection of seed points.

A digital speckle image matching method based on epipolar correction with large oblique fields of view is presented in this paper, which can effectively enhance the success rate and accuracy of speckle matching.

2. Epipolar Correction Theory

Epipolar correction is the theoretical foundation in this paper, thus the computational procedure of epipolar correction will be introduced first. The uncorrected epipolar geometric relation of a binocular camera is depicted in Figure 1(a), wherein P denotes an arbitrary point in space. The corresponding image points of P on the left and right image planes are denoted as P_l and P_r respectively. O_l and O_r represent the optical centers of the left and right cameras, and the line connecting the optical centers is called the baseline. The intersection points of the baseline with the image planes are termed as epipoles e_l and e_r. The epipolar lines connect image point with its corresponding epipole on the same image plane, denoted as l_{P_l}, l_{P_r}. The purpose of epipolar line correction is to make the left and right epipolar line horizontally collinear. The left and right images are fell on the same imaging plane through reprojecting. The rectified binocular camera system is illustrated in Figure 1(b).

✉Liping Liu
liuliping_tj@163.com

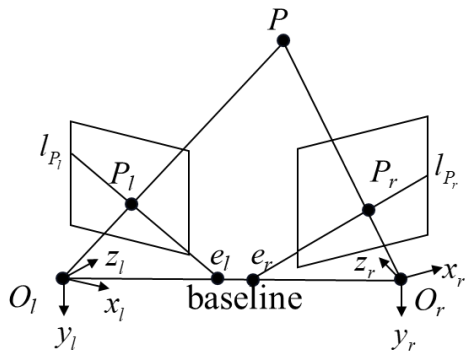

(a)Uncorrected binocular camera system

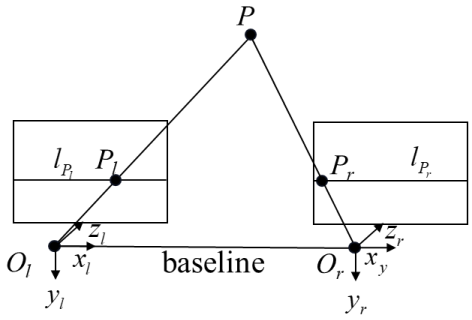

(b)Corrected binocular camera system

Fig. 1. Schematic of camera system before and after correction

The specific method for epipolar correction [15] is outlined as follows: Firstly, camera calibration is conducted to obtain the intrinsic and extrinsic parameters of the actual binocular camera system. Based on these parameters, the projection matrices for the left and right cameras can be computed. The projection matrices for the unrectified left and right cameras P_{o1} and P_{o2} are represented by $P_{o1} = \left[Q_{o1} \quad | q_{o1} \right]$, $P_{o2} = \left[Q_{o2} \quad | q_{o2} \right]$, and the coordinates c_1 and c_2 of the optical centers O_l and O_r are represented by $c_1 = -Q_{o1}^{-1} q_{o1}$, $c_2 = -Q_{o2}^{-1} q_{o2}$。

After correction, the left and right cameras should have the same orientation, meaning they possess an identical rotation matrix R. As a result, the projection matrices P_{n1} and P_{n2} of the rectified left and right cameras are respectively represented by

$$\begin{aligned} P_{n1} &= K_{n1}[R \mid -Rc_1] = \left[Q_{n1} \quad | q_{n1} \right] \\ P_{n2} &= K_{n2}[R \mid -Rc_2] = \left[Q_{n2} \quad | q_{n2} \right] \end{aligned} \tag{1}$$

Wherein K_{n1} and K_{n2} are the intrinsic parameters of the rectified cameras, and they can be set as required. It is necessary to ensure that the focal length and vertical translation of the intrinsic parameters for the left and right cameras are consistent.

The corrected rotation matrix R is constructed. The optical center coordinates of the corrected dual camera system and the original system remain unchanged. The line connecting O_l and O_r is used as the new X-axis. The rectified Y-axis is formed by taking the cross product of the original left camera's Z-axis with the new X-axis. Then, the corrected Y-axis is cross-multiplied with the corrected X-axis to obtain the corrected Z-axis. The corrected rotation matrix is expressed as follows:

✉Liping Liu
liuliping_tj@163.com

$$R = \begin{bmatrix} r_1^T \\ r_2^T \\ r_3^T \end{bmatrix} \tag{2}$$

Wherein $r_1 = (c1 - c2) / \| c1 - c2 \|$, $r_2 = k \times r_1$, $r_3 = r_1 \times r_2$, k represents the Z-axis of the original left camera.

The stereoscopic correction matrix is Constructed as:

$$\begin{cases} T_l = Q_{n1} Q_{o1}^{-1} \\ T_r = Q_{n2} Q_{o2}^{-1} \end{cases} \tag{3}$$

Wherein, T_l and T_r respectively represent the epipolar correction matrices for the left and right cameras.

Given that the homogeneous coordinates of a certain point on the unrectified left and right images are denoted as $\tilde{m}_{o1}$, $\tilde{m}_{o2}$, and their corresponding homogeneous coordinates on the rectified left and right images are $\tilde{m}_{n1}$, $\tilde{m}_{n2}$. So a relationship exists:

$$\begin{cases} \tilde{m}_{n1} = T_l \tilde{m}_{o1} \\ \tilde{m}_{n2} = T_r \tilde{m}_{o2} \end{cases} \tag{4}$$

The original image pixel coordinates corresponding to the whole pixel coordinates of the corrected image can be established by formula (4), and then the corrected left and right images can be calculated by interpolation.

3. The Principle of Digital Speckle Image Matching in Inclined Field of View Based on Epipolar Correction

After epipolar correction, the deformation in the left and right images is relatively small. It is assumed that the corrected left and right images only have rigid body deformation. Meanwhile, the images before and after correction can be correlated by the correction matrix. The virtual deformation model from the reference sub-region to the target sub-region is established by the relationship between the left and right images before and after correction. In this model, it is assumed that the reference sub-region deforms from the left image before correction to the left image after correction, then deforms to the right image after correction, and finally transforms to the right image before correction. In this way, the overall mapping shape function from the reference sub-region to the target sub-region can be decomposed into a combination of three shape functions. The independent estimation of the three shape functions after decomposition is easier than that of the original single shape function estimation. By solving the three shape functions separately, the overall mapping shape function can be estimated, and the initial value of deformation iteration calculated by using the estimated overall mapping shape function can be used to complete fine matching, for carrying out the subsequent deformation calculation.

Figure 2 shows the schematic diagram of the matching principle. It is assumed that the

✉Liping Liu
liuliping_tj@163.com

reference sub-region f converts the target subregion g by the shape function W. The form function W is decomposed as $W=W_rW_{l2r}W_l$. the physical meaning of the decomposition expression of W is that the reference sub-region f converts the reference sub-region f' by the shape function W_l, the reference sub-region f' then converts to the target sub-region g' by the shape function W_{l2r}, finally the target sub-region g' converts the target sub-region g by the shape function W_r.

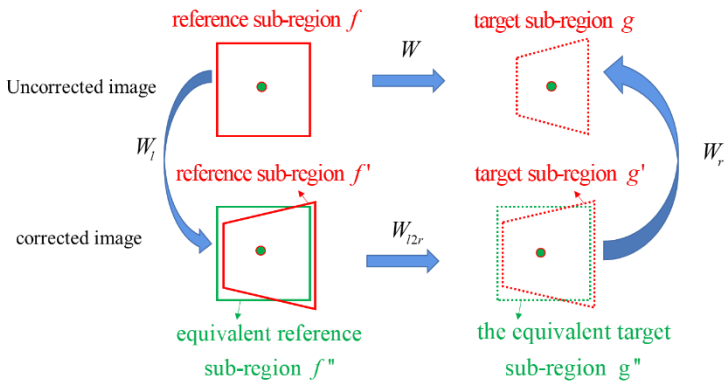

Fig. 2. Matching principle diagram

Consequently, the computation of the shape function W can be deconstructed into distinct processes focused on solving the shape functions W_l, W_{l2r}, and W_r. Given that the accurate calculation of these individual shape functions W_l, W_{l2r}, and W_r is often unnecessary, So we only make estimates. In the following sections, we will delve into the methods employed for estimating these shape functions W_l, W_{l2r}, and W_r.

Therefore, the process of calculating the shape function W can be divided into solving the shape functions W_l, W_{l2r}, and W_r respectively. As the shape functions W_l, W_{l2r}, and W_r usually cannot be absolute accurate calculation, and it is unnecessary to make absolutely precise calculations. So only estimation is done. The following will explain the estimation method of the shape functions W_l, W_{l2r}, and W_r.

W_l: The transformation from the reference sub-region f to the reference sub-region f' is completely realized by linear transformation of the correction matrix, assuming that the homogeneous coordinate of a point in the reference sub-region f is represented as $[x \quad y \quad 1]$, and the homogeneous coordinate of the corresponding point in the reference sub-region f' is represented as $[x' \quad y' \quad l]^T$. This relationship is established as illustrated in equation (4).

$$\begin{bmatrix} x' \\ y' \\ l \end{bmatrix} = T_l \begin{bmatrix} x \\ y \\ 1 \end{bmatrix} \tag{4}$$

The pixel coordinates of each point in the reference sub-region f' can be calculated by formula (4). So that the pixel coordinates of the corresponding points before and after the correction in the reference sub-region f and f' can be obtained. Then a first-order shape function W_l is used to characterize the deformation from reference sub-region f to reference sub-region f'. This is expressed as shown in equation (5).

✉Liping Liu
liuliping_tj@163.com

$$\begin{bmatrix} x_1' & x_2' & \dots & x_n' \\ y_1' & y_2' & \dots & y_n' \\ 1 & 1 & \dots & 1 \end{bmatrix} = \begin{bmatrix} 1+u_x & u_y & u \\ v_x & 1+v_y & v \\ 0 & 0 & 1 \end{bmatrix} \begin{bmatrix} \Delta x_1 & \Delta x_2 & \dots & \Delta x_n \\ \Delta y_1 & \Delta y_2 & \dots & \Delta y_n \\ 1 & 1 & \dots & 1 \end{bmatrix} \tag{5}$$

Let $X' = \begin{bmatrix} x_1' & x_2' & \dots & x_n' \\ y_1' & y_2' & \dots & y_n' \\ 1 & 1 & \dots & 1 \end{bmatrix}$, $W_l = \begin{bmatrix} 1+u_x & u_y & u \\ v_x & 1+v_y & v \\ 0 & 0 & 1 \end{bmatrix}$, $\Delta X = \begin{bmatrix} \Delta x_1 & \Delta x_2 & \dots & \Delta x_n \\ \Delta y_1 & \Delta y_2 & \dots & \Delta y_n \\ 1 & 1 & \dots & 1 \end{bmatrix}$, Wherein X' is a matrix composed of the global coordinates of points in the reference sub-region *f'*, W_l is the shape function, and ΔX is the matrix composed of the local coordinates of points in the reference sub-region *f*. Consequently, equation (5) is reformulated as follows:

$$X' = W_l \cdot \Delta X \tag{6}$$

The shape function W_l is calculated by the least squares method:

$$W_l = X' \cdot \Delta X^T \cdot (\Delta X \cdot \Delta X^T)^{-1} \tag{7}$$

Considering the calculation efficiency, it's unnecessary to use all points in the reference sub-region *f* for calculations. 16 points are taken at equal intervals centered on the midpoint of the reference sub-region *f*. The point selection scheme is depicted in Figure 3.

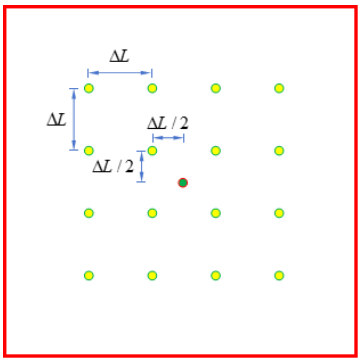

Fig. 3. point selection scheme of reference sub-region *f*

W_{l2r}: Assuming that there is only rigid body displacement between the reference sub-region *f'* and the target sub-region *g'*, then W_{l2r} can ignore the non-rigid shape variable, meaning that the strain can be ignored. The rationality of this assumption stems from the fact that the pixels of the corrected left and right image rows are aligned. Therefore, in theory, there should be no vertical deformation between the reference sub-region *f'* and the target sub-region *g'*, and then the reference sub-region *f'* and the target sub-region *g'* only experience deformation in the horizontal direction. In general, non-rigid deformations from the reference sub-region f' to the target sub-region g' are relatively small [14], and they can be ignored to a certain extent.

Through the Zero Mean Normalized Cross Correlation (ZNCC) whole-pixel matching algorithm, the midpoint coordinates of target sub-region *g'* are obtained. Calculate the translation component in W_{l2r} in this way. Since the reference sub-region *f'* isn't rectangular, direct computation is inconvenient. Thus, the matching process doesn't directly use the reference sub-region *f'*. Instead, the middle point of the reference sub-region *f'* is used to reconstruct an equivalent reference sub-

✉Liping Liu
liuliping_tj@163.com

region f'' which depicted by the green solid-line frame in Figure 2, which is used for matching in place of the reference sub-region f'.\\to replace the reference sub-region f' for matching. To prevent the computational speed loss resulting from interpolation during the reconstruction of sub-regions due to the midpoint of the equivalent reference sub-region f" being within the sub-pixel region, the midpoint coordinates of the reference sub-region f" can be rounded to the nearest integer values.\\\In order to avoid the problem of calculation speed loss caused by interpolation required for reconstruction of the subpixel region because the midpoint of the equivalent reference sub-region f'' is located in the sub-pixel region, the midpoint coordinates of the reference sub-region f" can be rounded to the nearest integer values.Since the ZNCC algorithm itself doesn't achieve sub-pixel accuracy, this approximation method has little impact on the precision of ZNCC matching. Since the small differences in shape between the equivalent reference sub-region f'' and the equivalent target sub-region g'', the ZNCC algorithm can search the correct peak correlation coefficient between the equivalent reference sub-region f" and the equivalent target sub-region g" with a high probability in theory.

W_r: Estimating W_r follows a similar process as estimating W_l. After obtaining the center coordinates of the target sub-region g' through matching, 16 points are selected following the point selection scheme shown in Figure 3. The pixel coordinates before and after correction are calculated for these 16 points. By replacing the relevant matrices in equations (4) to (6), W_r can be estimated.

Once the estimations for W_l, W_{l2r}, and W_r are completed, the estimation value for W can be calculated.

4. Experimental Validation and Result Analysis

In order to verify the effectiveness of digital speckle stereo matching algorithm based on epipolar correction in the inclined field of view, the experimental setup was built as shown in Fig. 4.

The self-made simulation device for uniform pressurization of aircraft fuselage skin was used to pressurize the Carbon Fiber Reinforced Polymer (CFRP) skin to measure the deformation of the skin. The stacking sequence of CFRP skin is $[0/45/-45/90/-45/45]_s$. The maximum applied pressure was 13.77 psi. The applied pressure mode was 0-13.77psi cyclic application. The experimental setup employed two monochrome industrial cameras (HT-SUA520-T), each with an effective resolution of 2592×1944 pixels. In this experiment, the position and posture of the left camera remained unchanged, while the position and posture of the right camera was changed to modify the inclination angle. Five different conditions were considered for the right camera's inclination angle: 24.2°, 34.2°, 41.15°, 47.3°, and 52.4°. The left image and the right images under various inclination angles was taken without pressurization as shown in Figure 5. The computer system is Windows 11, with an Intel(R) Core(TM) i7-11800H CPU@2. 30GHz, and 32GB of RAM. The code execution environment was Matlab 2022a.

✉Liping Liu
liuliping_tj@163.com

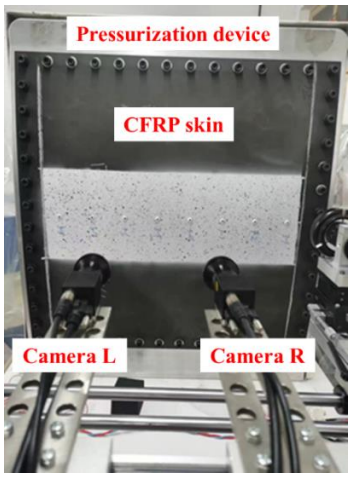

Fig. 4. Experimental setup

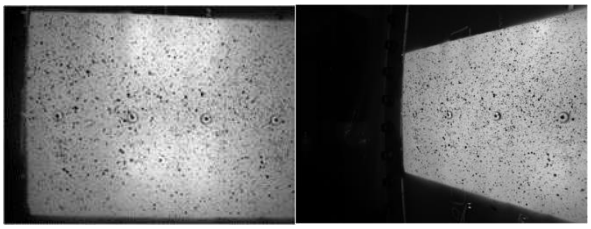

(a)Reference left image (d)41.2° right image

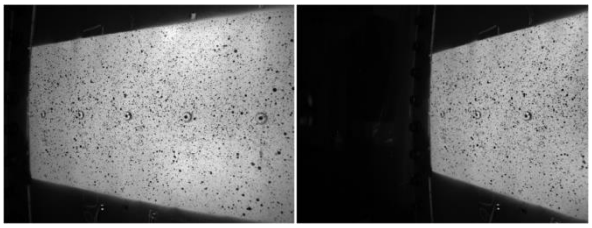

(b)24.2° right image (e)47.3° right image

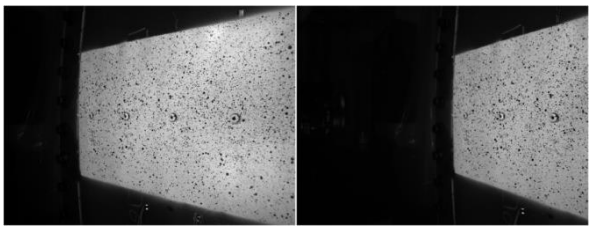

(c)34.2° right image (f)52.4° right image

Fig. 5. Left image and right image at different inclination angles

A necessary condition for DIC measurement is that the region to be measured exists in both the left and right images at the same time. To ensure that the region to be measured at different inclination angles meets this necessary condition, the measurement region was chosen as depicted in Figure 6.

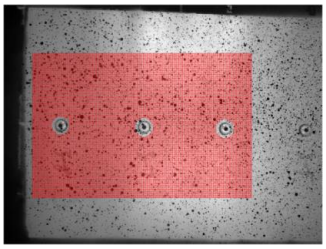

✉Liping Liu
liuliping_tj@163.com

Fig. 6. Measuring region

4.1 Rationality Validation of W_{l2r} Simplification

To demonstrate reasonableness of W_{l2r} simplified method, the ZNCC matching was performed on 20,632 detection points in the images after epipolar correction under five different camera inclination angles. The distribution of ZNCC coefficient peak values was analyzed. Table 1 is the statistical result of the mean values of ZNCC coefficient peak values for different conditions.

Table. 1 the mean values of ZNCC coefficient peak values for different conditions

Camera inclination Angle	24.2°	34.2°	41.2°	47.3°	52.4°
Mean values of ZNCC coefficient peak value	0.9457	0.9353	0.9097	0.8894	0.8744

As shown in Table 1, with the increase in camera inclination angle, the average of ZNCC correlation coefficient peak during ZNCC matching of the epipolar corrected images is lower. This phenomenon is primarily attributed to the compression of speckle features as the inclination angle increases, resulting in a degradation of speckle quality. It affects the accuracy of interpolation algorithms [16], leading to distortion in the rectified images. However, even at an inclination angle of 52.4°, the overall ZNCC correlation coefficient peaks still exhibit a relatively high level.

To validate that the epipolar corrected left and right images are more easily matched correctly, the distributions of correlation coefficient peaks during ZNCC matching before and after correction at an inclination angle of 52.4° are shown in Figure 7.

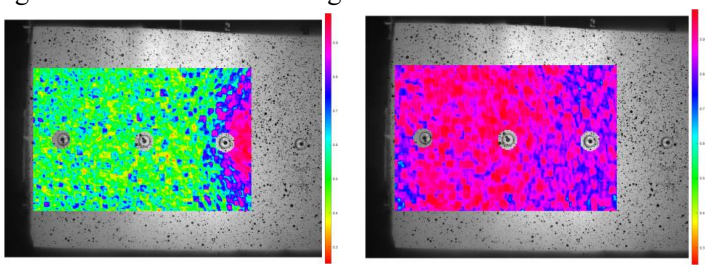

(a) Uncorrected peak distribution (b) Corrected peak distribution

Fig. 7. 52.4°Peak distribution of ZNCC matching correlation coefficient before and after correction at 52.4° inclination angle

As shown in Figure 7 (a), when conducting ZNCC matching on the unrectified left and right images, most sub-regions correlation coefficient peaks are less than 0.6. Only on the right side of the region to be measured, the correlation coefficient peaks exceed 0.8. Too small correlation coefficients pose challenges to the reliability of the matching result. Conversely, when performing ZNCC matching on the rectified left and right images, the correlation coefficient peaks in the whole region to be measured were mostly above 0.85. Higher correlation coefficients mean a greater level of reliability in the matching result. Therefore, conducting ZNCC matching on the epipolar corrected left and right images can improve the accuracy of the matching result.

These results prove that it is reasonable to ignore the non-rigid deformation of the reference sub-region f' and the target sub-region g' during the simplification process of matrix W_{l2r}. Consequently, it is reasonable to assume only existing rigid body displacement when estimating matrix W_{l2r}.

✉Liping Liu
liuliping_tj@163.com

4.2 Precision Analysis of Deformation Iterative Initial Value in epipolar Correction

Taking the case of a 52.4° inclination angle as an example, a sampling approach was adopted. Five points were randomly selected, the estimated deformation iterative initial values are compared with the final iteration result when NR method converges. The comparative result is shown in Table 2.

Table. 2 Precision comparison of initial value of deformation iteration for epipolar correction

Subarea number		1	2	3	4	5
	estimated value	1759.74	1455.70	1668.93	2273.61	2301.22
u	convergence value	1760.05	1455.72	1669.33	2273.99	2301.42
	deviation(%)	-0.0176	-0.0014	-0.024	-0.0167	-0.0087
	estimated value	918.39	756.26	1280.27	510	1056.76
v	convergence value	918.15	756.43	1280.24	510.63	1056.55
	deviation(%)	0.0261	-0.0225	0.0023	-0.1233	0.0199
	estimated value	-0.4211	-0.5745	-0.4696	-0.1043	-0.0856
u_x	convergence value	-0.3557	-0.5163	-0.4074	-0.0097	0.0123
	deviation(%)	18.39	11.27	15.27	975.26	-595.93
	estimated value	0.0053	0.0037	0.0048	0.0087	0.0089
u_y	convergence value	0.0019	-0.0020	0.0088	-0.0142	0.0112
	deviation(%)	178.95	-285.00	-45.45	-161.27	-20.54
	estimated value	-0.0181	-0.0525	0.0753	-0.1602	0.0242
v_x	convergence value	-0.0225	-0.0510	0.0889	-0.1804	0.0288
	deviation(%)	-19.56	2.94	-15.30	-11.20	-15.97
	estimated value	-0.2391	-0.3482	-0.2704	-0.0554	-0.0432
v_y	convergence value	-0.2385	-0.3397	-0.2703	-0.0531	-0.0424
	deviation(%)	0.2516	2.50	0.0370	4.33	1.89

The convergence values of u, v, u_x, u_y, v_x and v_y in Table 2 reflect the deformation amount of the corresponding component of the left and right images caused by different inclination angle of the left and right cameras. In u, v, u_x, u_y, v_x and v_y, the smaller the convergence value is, the smaller the deformation corresponding to the left and right images, and then it is more successful in NR fine matching. The larger the convergence value is, the larger the deformation corresponding to the left and right images. When NR fine matching is performed, it is more successful only when the estimated value of the initial deformation iteration is closer to the convergence value.

From Table 2, it is evident that the estimated deformation iterative initial values u, v, v_x, and v_y using the epipolar correction method are remarkably close to the convergence values. A large deviation between the estimated partial deformational iterative initial values of u_x and u_y and their convergent values is primarily attributed to ignoring certain strain deformation during simplifying of W_{l2r}. From Table 2, it can be observed that when the convergence value of u_x is relatively large, the estimated value of u_x is much closer to the convergence value of u_x than the zero value without estimation. The partial deformational iterative initial values which have a large relative deviation

✉Liping Liu
liuliping_tj@163.com

with the u_x and u_y convergence values have small values themselves, which almost does not affect the subsequent NR convergence. Furthermore, it can be seen from Table 2 that from the deformational iterative initial values after epipolar correction and the NR convergence values, the strain deformation of the image generated by camera inclination is mainly concentrated on u_x and v_y.

4.3 Success Rate Verification of Epipolar Correction Matching

The out-of-plane displacement field of the skin measured under different camera inclination angles is shown in Figure 8. The E_{xx} strain field is shown in Figure 9.

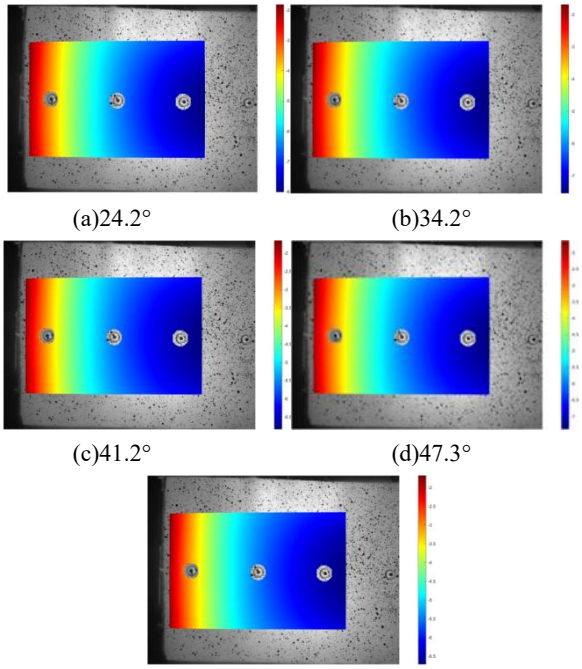

Fig. 8. out-of-plane displacement field of the skin

As shown in Figure 7, it is evident that the epipolar correction matching method proposed in this paper can be well completed the stereo matching under all five camera inclination angle conditions. Even at the case of extreme inclination like 52.4°, the matching of all measuring points is still successfully realized, and the matching success rate is as high as 100%.

In Figure 8, the maximum E_{xx} strain under different camera inclination angle is shown in Table 3. The maximum deviation of E_{xx} strain values among the five conditions does not exceed 3. 4%. It indicates that the calculated strain field maintains a high level of consistency. Because the strain is more sensitive to deviation, the highly consistent strain field shows that the digital speckle matching method based on epipolar correction in inclined field of view can guarantee sufficient strain measurement accuracy under the condition of small camera inclination angle and large camera inclination angle.

Table. 3. The maximum E_{xx} strain under different camera inclination angle

inclination angle	24.2°	34.2°	41.15°	47.3°	52.4°
E_{xx}	3771	3709	3888	3833	3902

✉Liping Liu
liuliping_tj@163.com

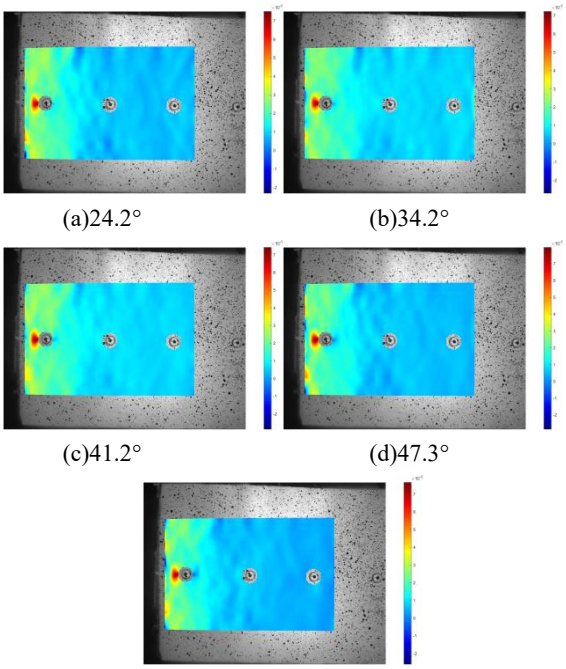

(a)24.2° (b)34.2°

(c)41.2° (d)47.3°

（e）52.4°

Fig. 9. Exx strain field

5.Conclusion

A digital speckle stereo matching method based on epipolar correction is proposed in this paper to address the issue of challenge about speckle image matching aiming at inclined fields of view. Based on the relationship between the left and right images before and after epipolar correction, a virtual mapping model from the reference sub-region to the target sub-region was established, and the overall mapping function from the reference sub-region to the target sub-region was decomposed into three shape functions. The three shape functions were estimated by the virtual mapping model, and then the three shape functions were reconstructed to obtain the deformational iterative initial values. The NR convergence is more easily realized by using the obtained deformational iterative initial values, thus improving the matching success rate and matching accuracy.

This research indicates that using the digital speckle stereo matching method based on epipolar correction results in the maximum deviation of E_{xx} strain values is no more than 3.4% under different camera inclination angles, and the calculated strain field is highly consistent.

Funding

This work was supported by the Tianjin Municipal Science and Technology Bureau (21JCYBJC00710).

CRediT authorship contribution statement

Liping Liu: Conceptualization. **Boya Niu:** Investigation. **Zhuo Xu:** Software. **Songyang Zhang:** Writing – original draft. **Zhaoyu Shao:** Writing – review & editing. **Xinyu Wang:** Validation.

✉Liping Liu
liuliping_tj@163.com

Declaration of Competing Interest

The authors declare the following financial interests/personal relationships which may be considered as potential competing interests:

Liping Liu has patent #CN202310496200.X issued to China National Intellectual Property Administration. If there are other authors, they declare that they have no known competing financial interests or personal relationships that could have appeared to influence the work reported in this paper.

Data availability

Data will be made available on request.

References

[1] PETERSW H. Digital Imaging Technique in Experimental[J]. Optical Engineering, 1982, 21 (3) : 427-431.

[2] Li LG, Liang J, Guo X, et al. Full-field wing deformation measurement scheme for in-flight cantilever monoplane based on 3D digital image correlation[J]. Meas Sci Tech-nol 2014, 25(6): 065202 .

[3] Wenjin Sun, Aibing Jin, Shuliang Wang, et al. Study on sandstone split mechanical properties under high temperature based on the DIC technology[J]. Rock and Soil Mechanics, 2021, 42(02): 511-518.

[4] Palanca M, Tozzi G, Cristofolini L. The use of digital image correlation in the biomechanical area: a review[J]. International Biomechanics, 2016, 3(1):1-21.

[5] Banfu Yan, Derui Li, Guanya Xu, et al. Structural Deformation Test Based on Fast Digital Image Correlation and Regularization Smoothing Techniques[J]. China Journal of Highway and Transport, 2020, 33(09):193-205.

[6] Yuehua Cheng, Hao Wu, Yijiang Xue, et al. Application of high-speed 3D-DICmeasurement technology in perforation test of armor steel[J]. Explosion and Shock Waves, 2022,42(10): 111-125.

[7] Zhangliang Wu, Changku Sun, Zhongdong Yang. Design and analysis of structural parameters of vision measurement sensor system[J]. optoelectronic component, 2009, 36(12): 56-61+90.

[8] Bing Pan, Kemao, et al. Two-dimensional digital image correlation for in-plane displacement and strain measurement: a review[J]. Measurement Science and Technology, 2009, 20(6): 062001.

[9] Vendroux G, Knauss WG. Submicron deformation field measurements: Part 2. Improved digital image correlation[J]. Experimental Mechanics, 1998, 38(2): 86-92.

[10] Yi Liu. Research on Displacement and Strain Measurement of Rotating Object Based on Digital Image Correlation[D].Jiang xi: East China Jiaotong University,2021:24-25.

[11] Bin Wei, Jin Liang, Jie Li, et al. 3D full-field wing deformation measurement method for large high-wing airplanes[J]. Acta Aeronautica et Astronautica Sinica, 2017,38(7):172-181.

[12] Hongying Zhang, Zhijing Yu. Initial displacement estimation method for speckle image based

✉Liping Liu
liuliping_tj@163.com

on marker matching [J]. Acta Optica Sinica,2017, 37(3): 0303001.(in Chinese)

[13] Meitu Ye, Jin Liang, Leigang Li, et al. Discretization matching of weakly correlated speckle images in oblique field of view[J]. Optics and Precision Engineering, 2021, 29(09): 2235-2246.

[14] Fusiello A, Trucco E, Verri A. A compact algorithm for rectification of stereo pairs[J]. Machine Vision and Applications, 2000, 12(1): 16-22.

[15] ShaoHui Song. Research on Dynamic Deformation Measurement Method of Binocular Stereoscopic Vision Based on DSCM[D].Tian jin: Tianjin University,2021.

[16] SU Yong, ZHANG Qingchuan, XU Xiaohai, et al. Theoretical estimation of interpolation bias error in digital image correlation[J].Chinese Journal of Theoretical and Applied Mechanics, 2016, 48(02): 495-510.

✉Liping Liu
liuliping_tj@163.com